Brillouin and Kerr nonlinearities of a low-index silicon oxynitride platform 🄴🄿

Kaixuan Ye ⓘ ; Yvan Klaver ⓘ ; Oscar A. Jimenez Gordillo ⓘ ; Roel Botter ⓘ ; Okky Daulay ⓘ ;
Francesco Morichetti ⓘ ; Andrea Melloni ⓘ ; David Marpaung ✉ ⓘ

Check for updates

View Online   Export Citation   CrossMark

AIP Publishing

Brillouin and Kerr nonlinearities of a low-index silicon oxynitride platform EP

View Online   Export Citation   CrossMark

Kaixuan Ye,[1] Yvan Klaver,[1] Oscar A. Jimenez Gordillo,[2] Roel Botter,[1] Okky Daulay,[1]
Francesco Morichetti,[2] Andrea Melloni,[2] and David Marpaung[1,a]

AFFILIATIONS

[1] Nonlinear Nanophotonics, MESA+ Institute of Nanotechnology, University of Twente, Enschede, The Netherlands
[2] Dipartimento di Elettronica, Informazione e Bioingegneria (DEIB), Politecnico di Milano, Italy

[a] Author to whom correspondence should be addressed: david.marpaung@utwente.nl

ABSTRACT

Nonlinear optical effects including stimulated Brillouin scattering (SBS) and four-wave mixing (FWM) play an important role in microwave photonics, optical frequency combs, and quantum photonics. Harnessing SBS and FWM in a low-loss and versatile integrated platform would open the path to build large-scale Brillouin/Kerr-based photonic integrated circuits. In this letter, we investigate the Brillouin and Kerr properties of a low-index ($n = 1.513$ @ 1550 nm) silicon oxynitride (SiON) platform. We observed, for the first time, backward Brillouin scattering in SiON waveguides with a Brillouin gain coefficient of 0.3 $\mathrm{m^{-1}\ W^{-1}}$, which can potentially be increased to 0.95 $\mathrm{m^{-1}\ W^{-1}}$ by just tailoring the waveguide cross section. We also performed FWM experiments in SiON rings and obtained the nonlinear parameter γ of 0.02 $\mathrm{m^{-1}\ W^{-1}}$. Our results point to a low-loss and low-index photonic integrated platform that is both Brillouin and Kerr active.

I. INTRODUCTION

Stimulated Brillouin scattering (SBS), which is an interaction between optical and acoustic waves, is currently revolutionizing photonic integrated circuit designs.[1–8] Featuring a narrow-band (tens of MHz) gain resonance shifted around tens of GHz away from the pump light, the on-chip SBS plays a significant role in microwave photonics,[9–11] narrow-linewidth integrated lasers,[7,12,13] and on-chip nonreciprocal light propagation.[3,14]

An efficient on-chip SBS process requires simultaneous guiding of both the optical and gigahertz acoustic waves in a waveguide, making it challenging to realize on most integrated platforms. Several encouraging results have been demonstrated recently on various platforms, including chalcogenide,[2] silicon,[5] doped silica,[15] aluminum gallium arsenide,[16] and aluminum nitride.[17] In addition, SBS has also been observed in silicon nitride-based waveguides,[7,8,18] opening the pathway to intersect Brillouin scattering with Kerr nonlinearities in low-loss and mature platforms.

Silicon oxynitride (SiON) is another highly-developed integrated platform that has appealing properties, including low propagation loss, a wide transparency window, the absence of multiphoton absorption effects, and stress-free fabrication.[19,20]

The optical and mechanical properties of SiON could be tuned continuously between those of $\mathrm{SiO_2}$ and $\mathrm{Si_3N_4}$ at different nitrogen/oxygen (N/O) ratios.[21,22] For example, a variety of SiON known as Hydex ($n = 1.7$ @ 1550 nm) has been widely used for Kerr-based nonlinear optic applications including optical frequency comb,[23] optical neural network,[24] and quantum photonics.[25] A slightly higher index of SiON ($n = 1.83$ @ 1550 nm) was also proposed in Refs. 20 and 26 for Kerr-based applications. In both cases, the SiON platforms have a refractive index close to that of silicon nitride ($n = 1.98$ @ 1550 nm) instead of silicon oxide ($n = 1.45$ @ 1550 nm). The relatively high refractive index induces a high nonlinear index, making it useful for Kerr-based nonlinear optic applications.

However, from the Brillouin perspective, a high refractive index SiON is less attractive due to the high content of nitrogen, which leads to a meager photoelastic coefficient p_{12} because of the weak p_{12} of the $\mathrm{Si_3N_4}$.[18] Moreover, high-index SiON also has similar mechanical properties to $\mathrm{Si_3N_4}$, such as high acoustic velocity that prevents acoustic confinement when cladded with $\mathrm{SiO_2}$.[7,8,18]

In this paper, we investigate the Brillouin and Kerr properties of a SiON integrated platform with a relatively lower refractive index ($n = 1.513$ @ 1550 nm). Contrasting to the SiON platforms

mentioned earlier, the SiON platform investigated here has a larger photoelastic coefficient p_{12}, a lower acoustic velocity, and a larger cross section, all of which lead to an enhanced SBS effect. We experimentally observed, for the first time to our knowledge, backward Brillouin scattering in SiON waveguides. We also characterized the Brillouin gain coefficient g_b of the SiON waveguides with different widths. We found out that the g_b of this SiON waveguide can potentially be increased to 0.9 m^{-1} W^{-1} by simply tailoring the waveguide cross section. This sufficiently large Brillouin gain coefficient, together with the low propagation loss, makes it possible to generate decent SBS gain for a plethora of Brillouin-based applications on this SiON platform.

Furthermore, we also measured the nonlinear parameter γ and nonlinear index n_2 of this SiON platform through four wave mixing (FWM) experiments in a ring resonator. While the measured γ is an order of magnitude lower when compared to that of high-index SiON, we expect that with lower losses and higher pump power, the unique interplay between the SBS and Kerr effect, such as a Brillouin-assisted Kerr frequency comb,[27,28] could be observed in this integrated platform.

II. RESULTS

We performed the backward Brillouin scattering and four-wave mixing experiments in 5 cm straight waveguides and microring resonators, respectively, as shown in Fig. 1(a). The cross section of this platform is shown in Fig. 1(b).[29,30] The 2.2 m-thick SiON layer has a refractive index n of 1.513 at 1550 nm [nitrogen content N/(N + O) is 0.14]. The refractive index contrast Δn between the core and the

cladding is 4.4%, enabling a bending radius of 600 m with negligible radiation losses.

The SiON film is deposited by Plasma Enhanced Chemical Vapor Deposition (PECVD) on a 15-m-thick silicon dioxide film thermally grown on a silicon substrate. After the SiON PECVD process, an annealing treatment for 4 h at 1175 °C in the N$_2$ and O$_2$ atmospheres is conducted to reduce both material losses induced by residual N–H bonds and stresses. The waveguides are then patterned by contact photolithography, followed by a reactive ion etching step on the SiON film. A 7-m-thick layer of borophosphosilicate glass (BPSG) is employed as the upper-cladding material. This low viscosity glass permits covering the waveguides completely without any voids that would generate scattering and additional losses.

Figure 1(c) shows a photograph of the microring resonators in this platform with a free spectral range (FSR) of 50 GHz and coupling coefficients varying from 0.05 to 0.8. Figure 1(d) shows a photograph of several groups of 5 cm straight waveguides with different widths. The measured propagation loss of those straight waveguides is 0.25 dB/cm with a coupling loss to lensed-tip fibers of ~3 dB/facet.

A. Backward Brillouin scattering in SiON waveguides

We developed a finite element model[8] in COMSOL to estimate the SBS response of the SiON waveguides. We take the bottom and upper cladding as the same material in our model since the BPSG glass and the SiO$_2$ have similar optical and mechanical properties.[31,32] The simulated optical field and the corresponding acoustic response of the 2.2 m-wide SiON waveguide are shown in Figs. 2(a) and 2(b), respectively. The optical field is well confined around the SiON core area because of the total internal reflection (TIR). However, the TIR condition does not hold for the acoustic response because the acoustic velocity of the SiON (~6.2 km/s) is higher than that of the SiO$_2$ (~5.9 km/s). As a result, part of the acoustic field would leak into the cladding, as shown in Fig. 2(b). Nevertheless, most of the acoustic field still remains inside the SiON core because of the relatively large cross section area.[33] This results in a large overlap between the optical and acoustic fields, which leads to an improved Brillouin gain coefficient. Material properties applied in our model and extensive simulation results are included in the supplementary material.

To verify the simulation results, we characterized the backward Brillouin scattering responses of the SiON waveguides with a pump-probe experimental apparatus.[8,18] The pump and probe light are intensity-modulated and coupled into the opposite facets of the waveguide. We keep the pump frequency fixed at 1561 nm while sweeping the probe at frequencies down-shifted from the pump. When the frequency difference between the pump and the probe is close to the Brillouin frequency shift of the SiON waveguide, the probe will experience the SBS gain, and a peak will be detected at the lock-in amplifier (see the supplementary material for more details about the Brillouin characterizations).

Several 5 cm-long SiON straight waveguides are characterized to investigate the influence of waveguide width on the Brillouin gain spectra. The measured Brillouin gain spectra of the 2.0, 2.2, 2.3, 2.4, 2.6, and 3.5 m-wide waveguides are shown in Figs. 2(c)–2(h), respectively. All waveguides show a clear Brillouin gain peak well
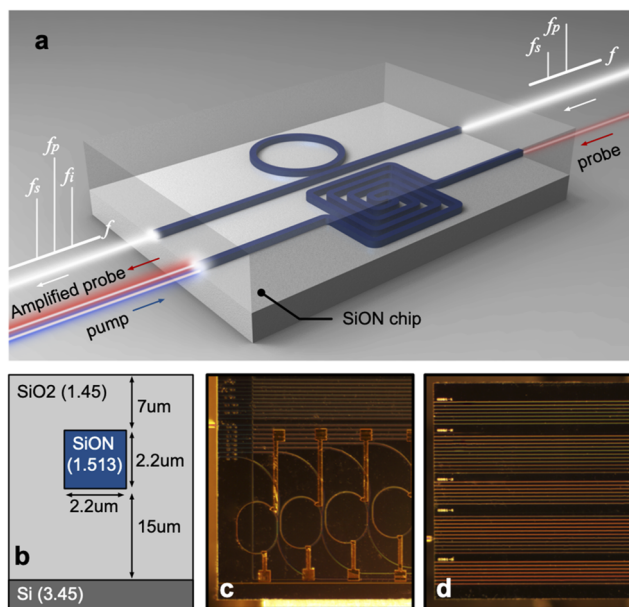

FIG. 1. (a) Artistic representation of the SiON waveguides, showing the four wave mixing process in an all-pass microring resonator and the backward stimulated Brillouin scattering (SBS) in a spiral waveguide. (b) The cross section of the SiON platform in our work. (c) The chip photograph of the SiON microring resonators with an FSR of 50 GHz. (d) The chip photograph of the 5 cm SiON straight waveguide.
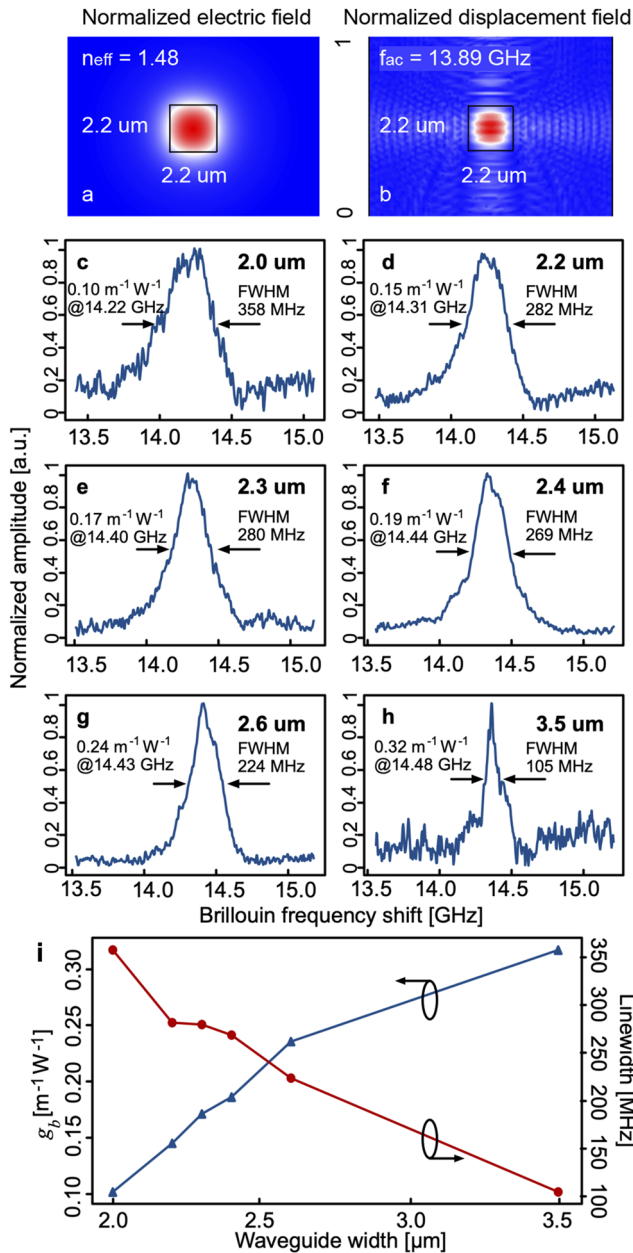
FIG. 2. (a) Simulated optical mode of the SiON waveguide. (b) Simulated acoustic response of the SiON waveguide. (c)–(h) Measured Brillouin gain spectra of the 2.0, 2.2, 2.3, 2.4, 2.6, and 3.5 m-wide SiON waveguides, respectively. (i) Brillouin gain coefficients and linewidth of the SiON waveguides with different widths.

above the noise floor with the Brillouin frequency shift increasing from 14.22 GHz for the 2.0 m-wide waveguide to 14.48 GHz for the 3.5 m-wide waveguide. The discrepancy between the experiment and simulation in Brillouin frequency shift is mainly caused by a lack of knowledge about the exact mechanical properties of the SiON. Figure 2(i) plots the measured Brillouin gain coefficient g_b and the linewidth of the SiON waveguides with different widths

(see the supplementary material for more details about the Brillouin gain coefficient calculation). The Brillouin gain coefficient g_b increases from 0.1 to 0.32 m^{-1} W^{-1} when the waveguide width increases from 2.0 to 3.5 m. In the meantime, the linewidth of the peak decreases from 358 to 105 MHz. The increasing Brillouin gain coefficient and the narrowing of the linewidth indicate improved acoustic confinement when the SiON waveguides become wider.

The Brillouin gain coefficient can be further increased by optimizing the cross-section of the waveguide (maintaining the core as a rectangular shape) through a genetic algorithm.[8] Figures 3(a) and 3(b) show the simulated optical mode and the acoustic response of the optimized SiON waveguide for SBS. The dimension of such a waveguide is 3.6×3.0 m^2 with a top cladding of 6 m and a bottom cladding of 12 m. The optimized cross-section is a trade-off between the optical mode area and the overlap between the optical and displacement fields. Compared to waveguides measured in this work, less acoustic field is scattered into the cladding, while the optical field is still well confined and relatively small in the optimized waveguide structure. The Brillouin gain spectrum of the optimized waveguide structure is shown in Fig. 3(c). The simulated peak Brillouin gain coefficient of this waveguide is 0.9 m^{-1} W^{-1}, which is 3× higher than the waveguide structure measured in this work. Furthermore, the propagation loss on this SiON platform can also be significantly lowered by reducing sidewall roughness and improving the thermal annealing process,[30] allowing for a longer effective waveguide length for the SBS process. Figure 3(d) estimates the SBS gain of both the measured and the optimized SiON waveguides with different propagation losses. The optimized Brillouin gain coefficient, along with the improved propagation loss, can enhance the SBS gain from less than 0.5 dB to nearly 1.5 dB for a 60 cm waveguide. The actual SBS gain from the optimized waveguide might be lower than our estimations, as indicated by the discrepancy between the measurement and simulation results; nevertheless, it would still be sufficient for applications like SBS-based narrow-bandwidth microwave photonic notch filters.[8,10]
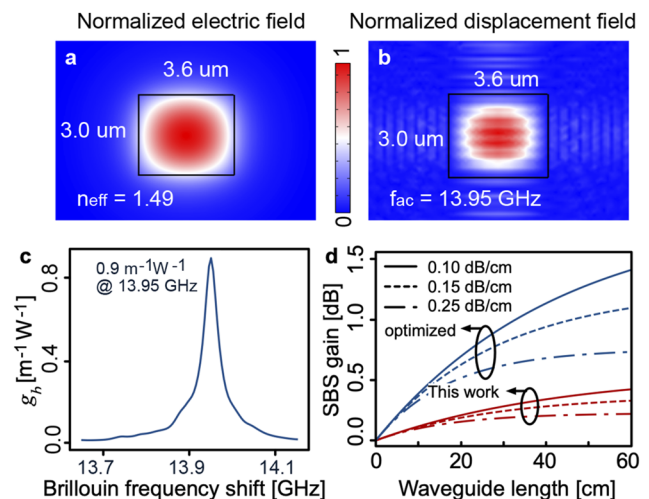

FIG. 3. (a) Simulated optical mode, (b) simulated acoustic response, (c) simulated Brillouin gain spectrum of the optimized SiON waveguide. (d) Estimated SBS gain from the optimized and current SiON waveguides.
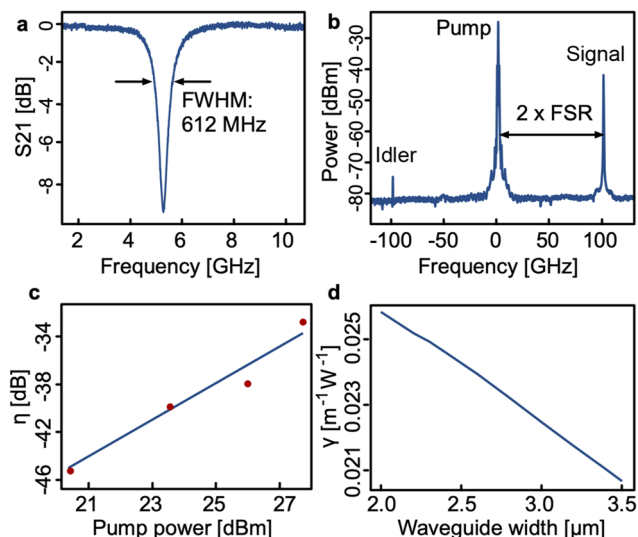
FIG. 4. (a) Measured resonance response of the SiON ring resonator. (b) Measured four-wave mixing response of the SiON ring resonator. (c) Conversion efficiency of the four wave mixing at different pump powers. (d) The estimated nonlinear parameter γ of the SiON waveguides with different widths.

B. Four-wave mixing in SiON waveguides

We further investigate the Kerr nonlinearities of this SiON platform. Hig-index SiON platforms are widely used for Kerr-based nonlinear optics applications because of the relatively large nonlinear parameter γ.[19] However, the nonlinear parameter γ is highly dependent on the refractive index and the geometry of the waveguide. The SiON waveguide in this work has a relatively lower refractive index and a larger cross section compared with other SiON platforms,[19,20] and the nonlinear index n_2 and nonlinear parameter γ of the SiON waveguide in this platform have never been characterized before.

We devised a four-wave mixing (FWM) experiment for nonlinear parameter characterization. Because of the limited effective length of the available samples, the FWM conversion efficiency of the straight waveguide is comparable with that of the fiber pigtails, making it difficult to accurately measure the n_2 and the γ. We use the all-pass ring resonators to enhance the FWM in the SiON waveguide

so that the contribution from fibers in the setup can be neglected.[34] The ring resonator applied in our experiment is made of a 2.2 m-wide SiON waveguide, and it has a free spectral range (FSR) of 50 GHz and a power coupling coefficient of 0.05. The pump laser is locked close to the resonance of the ring resonator to mitigate the thermal influence on the ring resonator. The probe laser is set close to 2× FSR away from the pump signal and is combined with the pump light with a 99:1 coupler. The combined pump and probe are coupled into the all-pass ring resonator with a lensed fiber with a spot size of 2 m. The signal is then coupled out of the chip and sent to the optical spectrum analyzer to measure the conversion efficiency from the probe to the signal (see the supplementary material for details of the FWM experiment).

To determine the field enhancement factor of the FWM process in the ring resonator, we first characterized the resonance response of the ring resonator with a vector network analyzer, as shown in Fig. 4(a) (see the supplementary material for details of the characterization). The measured full-width at half-maximum (FWHM) is 612 MHz with an extinction ratio of 8.9 dB, corresponding to a loaded Q-factor of 330 000 and a propagation loss of 0.27 dB/cm. Figure 4(b) shows the measured FWM response of the 50 GHz SiON ring resonator. A clear peak is shown at 2× FSR down-shifted from the pump frequency, which is the signal generated from the FWM process between the pump and idler in the ring resonator.

The nonlinear index n_2 and nonlinear parameter γ of the SiON waveguide in this platform can be estimated from the conversion efficiency between the idler and the signal (see the supplementary material for details of the calculation). Figure 4(c) shows the measured conversion efficiency of the FWM process at different pump powers. Based on this measurement, the calculated γ and n_2 of the 2.2 m-wide SiON waveguide are 0.024 m^{-1} W^{-1} and 4.16×10^{-20} m^2/W, respectively. We also estimated the nonlinear parameter γ of the SiON waveguides with different widths based on the measured value of n_2, as shown in Fig. 4(d). The γ decreases from around 0.025 to 0.020 m^{-1} W^{-1} when the waveguide width increases from 2.0 to 3.5 m.

III. DISCUSSION

For Brillouin-Kerr interactions, the balance between the nonlinearities needs to be considered. In this work, we have listed the Brillouin and Kerr properties of SiO$_2$, different types of Si$_3$N$_4$ waveguides, the Hydex waveguide, and the SiON waveguide in Table I.

TABLE I. Brillouin and Kerr nonlinearities of different Si$_3$N$_4$ based platforms.

	n_{eff}	n_2 (m^2/W)	γ (m^{-1} W^{-1})	g_b (m^{-1} W^{-1})	Ω_b (GHz)	$\Delta\nu_b$ (MHz)	Propagation loss (dB/cm)
SiO$_2$[35]	1.45	2.6×10^{-20}	0.00145	0.14	10.87	20	2×10^{-6}
Dilute Si$_3$N$_4$[7,36,37]	1.48	9×10^{-20}	0.285	0.1	10.9	143	0.004
Double-stripe Si$_3$N$_4$[8,38]	1.53	1.3×10^{-19}	0.23	0.4	12.93	130	0.19
Thick Si$_3$N$_4$[18]	1.85	2.5×10^{-19}	0.84	0.07	25	517	<0.1
Hydex[19]	1.65	1.3×10^{-19}	0.24	⋯	⋯	⋯	0.07
SiON (this work)	1.48	4.16×10^{-20}	0.020	0.32	14.48	105	0.25

The thick Si_3N_4 waveguide[18] has a large Kerr nonlinear parameter γ but negligible g_b, making it promising for Kerr-only applications. However, in Brillouin-Kerr microcavities, it is generally preferred to have a larger Brillouin gain, as it is easier to inhibit cascading or other unwanted interactions via mode manipulation. The SiON waveguides reported here have an order of magnitude larger Brillouin gain compared to Kerr nonlinearity. This g_b/γ ratio is similar to the previous demonstration of Brillouin-assisted Kerr frequency combs in Refs. 27 and 28, showing the potential to realize it on an integrated platform.

In conclusion, we have investigated the Brillouin and Kerr properties of a SiON integrated platform with a relatively low refractive index. We observed, for the first time, the backward Brillouin scattering response of the SiON waveguides. We also measured its nonlinear index n_2 and nonlinear parameter γ. These SiON waveguides can be fabricated on a versatile and low-loss integrated platform and can potentially lead to a plethora of Brillouin and Kerr-based applications, including narrow-bandwidth microwave photonic filters, narrow-linewidth lasers, and optical frequency combs.

SUPPLEMENTARY MATERIAL

See the supplementary material for details of the Brillouin and Kerr characterizations.

ACKNOWLEDGMENTS

AUTHOR DECLARATIONS

Conflict of Interest

The authors have no conflicts to disclose.

Author Contributions

D.M. and K.Y. developed the concept and proposed the physical system. K.Y. and Y.K. developed and performed numerical simulations. K.Y. performed the Brillouin characterization with input from R.B., K.Y., and O.D. Y.K. and K.Y. performed the FWM experiments. O.A.J.G., F.M., and A.M. developed and fabricated the samples. K.Y., D.M., and Y.K. wrote the article. D.M. led and supervised the entire project.

Kaixuan Ye: Conceptualization (equal); Data curation (equal); Formal analysis (equal); Investigation (equal); Software (equal); Visualization (equal); Writing – original draft (equal). **Yvan Klaver**: Data curation (equal); Investigation (equal); Writing – original draft (equal). **Oscar A. Jimenez Gordillo**: Methodology (equal); Resources (equal). **Roel Botter**: Investigation (equal);
Methodology (equal). **Okky Daulay**: Investigation (equal); Methodology (equal). **Francesco Morichetti**: Investigation (equal); Methodology (equal); Resources (equal). **Andrea Melloni**: Investigation (equal); Methodology (equal); Resources (equal). **David Marpaung**: Conceptualization (equal); Formal analysis (equal); Funding acquisition (equal); Project administration (equal); Supervision (equal); Writing – original draft (equal).

DATA AVAILABILITY

The data that support the findings of this study are available from the corresponding author upon reasonable request.

REFERENCES

[1]B. J. Eggleton, C. G. Poulton, P. T. Rakich, M. J. Steel, and G. Bahl, "Brillouin integrated photonics," Nat. Photonics **13**, 664 (2019).

[2]R. Pant, C. G. Poulton, D.-Y. Choi, H. Mcfarlane, S. Hile, E. Li, L. Thevenaz, B. Luther-Davies, S. J. Madden, and B. J. Eggleton, "On-chip stimulated Brillouin scattering," Opt. Express **19**, 8285–8290 (2011).

[3]E. A. Kittlaus, N. T. Otterstrom, P. Kharel, S. Gertler, and P. T. Rakich, "Non-reciprocal interband Brillouin modulation," Nat. Photonics **12**, 613–619 (2018).

[4]E. A. Kittlaus, N. T. Otterstrom, and P. T. Rakich, "On-chip inter-modal Brillouin scattering," Nat. Commun. **8**, 15819 (2017).

[5]E. A. Kittlaus, H. Shin, and P. T. Rakich, "Large Brillouin amplification in silicon," Nat. Photonics **10**, 463–467 (2016).

[6]P. T. Rakich, C. Reinke, R. Camacho, P. Davids, and Z. Wang, "Giant enhancement of stimulated Brillouin scattering in the subwavelength limit," Phys. Rev. X **2**, 011008 (2012).

[7]S. Gundavarapu, G. M. Brodnik, M. Puckett, T. Huffman, D. Bose, R. Behunin, J. Wu, T. Qiu, C. Pinho, N. Chauhan, J. Nohava, P. T. Rakich, K. D. Nelson, M. Salit, and D. J. Blumenthal, "Sub-hertz fundamental linewidth photonic integrated Brillouin laser," Nat. Photonics **13**, 60–67 (2018).

[8]R. Botter, K. Ye, Y. Klaver, R. Suryadharma, O. Daulay, G. Liu, J. van den Hoogen, L. Kanger, P. van der Slot, E. Klein, M. Hoekman, C. Roeloffzen, Y. Liu, and D. Marpaung, "Guided-acoustic stimulated Brillouin scattering in silicon nitride photonic circuits," Sci. Adv. **8**, eabq2196 (2022).

[9]D. Marpaung, J. Yao, and J. Capmany, "Integrated microwave photonics," Nat. Photonics **13**, 80–90 (2019).

[10]D. Marpaung, B. Morrison, M. Pagani, R. Pant, D.-Y. Choi, B. Luther-Davies, S. J. Madden, and B. J. Eggleton, "Low-power, chip-based stimulated Brillouin scattering microwave photonic filter with ultrahigh selectivity," Optica **2**, 76 (2015).

[11]L. McKay, M. Merklein, A. C. Bedoya, A. Choudhary, M. Jenkins, C. Middleton, A. Cramer, J. Devenport, A. Klee, R. DeSalvo, and B. J. Eggleton, "Brillouin-based phase shifter in a silicon waveguide," Optica **6**(7), 907–913 (2019).

[12]N. T. Otterstrom, R. O. Behunin, E. A. Kittlaus, Z. Wang, and P. T. Rakich, "A silicon Brillouin laser," Science **360**, 1113–1116 (2018).

[13]N. Chauhan, A. Isichenko, K. Liu, J. Wang, Q. Zhao, R. O. Behunin, P. T. Rakich, A. M. Jayich, C. Fertig, C. W. Hoyt, and D. J. Blumenthal, "Visible light photonic integrated Brillouin laser," Nat. Commun. **12**, 4685 (2021).

[14]J. Kim, M. C. Kuzyk, K. Han, H. Wang, and G. Bahl, "Non-reciprocal Brillouin scattering induced transparency," Nat. Phys. **11**, 275–280 (2015).

[15]S. Li, X. Li, W. Zhang, J. Chen, and W. Zou, "Investigation of Brillouin properties in high-loss doped silica waveguides by comparison experiment," IEEE Photonics Technol. Lett. **32**, 948–951 (2020).

[16]W. Jin, L. Chang, W. Xie, H. Shu, J. D. Peters, X. Wang, and J. E. Bowers, "Stimulated Brillouin scattering in AlGaAs on insulator waveguides," in Conference on Lasers and Electro-Optics (IEEE, 2020), paper SM4L.7.

[17]Q. Liu, H. Li, and M. Li, "Electromechanical Brillouin scattering in integrated optomechanical waveguides," Optica **6**, 778–785 (2019).

[18]F. Gyger, J. Liu, F. Yang, J. He, A. S. Raja, R. N. Wang, S. A. Bhave, T. J. Kippenberg, and L. Thévenaz, "Observation of stimulated Brillouin scattering in silicon nitride integrated waveguides," Phys. Rev. Lett. **124**, 013902 (2020).

[19]D. J. Moss, R. Morandotti, A. L. Gaeta, and M. Lipson, "New CMOS-compatible platforms based on silicon nitride and Hydex for nonlinear optics," Nat. Photonics **7**, 597–607 (2013).

[20]A. Trenti, M. Borghi, S. Biasi, M. Ghulinyan, F. Ramiro-Manzano, G. Pucker, and L. Pavesi, "Thermo-optic coefficient and nonlinear refractive index of silicon oxynitride waveguides," AIP Adv. **8**, 025311 (2018).

[21]T. Bååk, "Silicon oxynitride; a material for GRIN optics," Appl. Opt. **21**(6), 1069–1072 (1982).

[22]H. T. Grahn, H. J. Maris, J. Tauc, and K. S. Hatton, "Elastic properties of silicon oxynitride films determined by picosecond acoustics," Appl. Phys. Lett. **53**, 2281 (1998).

[23]M. Rowley, P.-H. Hanzard, A. Cutrona, H. Bao, S. T. Chu, B. E. Little, R. Morandotti, D. J. Moss, G.-L. Oppo, J. S. Totero Gongora, M. Peccianti, and A. Pasquazi, "Self-emergence of robust solitons in a microcavity," Nature **608**(7922), 303–309 (2022).

[24]X. Xu, M. Tan, B. Corcoran, J. Wu, A. Boes, T. G. Nguyen, S. T. Chu, B. E. Little, D. G. Hicks, R. Morandotti, A. Mitchell, and D. J. Moss, "11 TOPS photonic convolutional accelerator for optical neural networks," Nature **589**(7840), 44–51 (2021).

[25]C. Reimer, M. Kues, P. Roztocki, B. Wetzel, F. Grazioso, B. E. Little, S. T. Chu, T. Johnston, Y. Bromberg, L. Caspani, D. J. Moss, and R. Morandotti, "Generation of multiphoton entangled quantum states by means of integrated frequency combs," Science **351**, 1176–1180 (2016).

[26]G. Piccoli, M. Sanna, M. Borghi, L. Pavesi, and M. Ghulinyan, "Silicon oxynitride platform for linear and nonlinear photonics at NIR wavelengths," Opt. Mater. Express **12**, 3551 (2022).

[27]Y. Bai, M. Zhang, Q. Shi, S. Ding, Y. Qin, Z. Xie, X. Jiang, and M. Xiao, "Brillouin-Kerr soliton frequency combs in an optical microresonator," Phys. Rev. Lett. **126**, 063901 (2021).

[28]M. Nie, K. Jia, Y. Xie, S. Zhu, Z. Xie, and S. W. Huang, "Synthesized spatiotemporal mode-locking and photonic flywheel in multimode mesoresonators," Nat. Commun. **13**(1), 6395 (2022).

[29]F. Morichetti, S. Grillanda, S. Manandhar, V. Shutthanandan, L. Kimerling, A. Melloni, and A. M. Agarwal, "Alpha radiation effects on silicon oxynitride waveguides," ACS Photonics **3**, 1569–1574 (2016).

[30]F. Morichetti, A. Melloni, A. Breda, A. Canciamilla, C. Ferrari, and M. Martinelli, "A reconfigurable architecture for continuously variable optical slow-wave delay lines," Opt. Express **15**, 17273–17282 (2007).

[31]M. Gartner, M. Modreanu, S. Bosch, and T. Stoica, "Optical characterization of dielectric borophosphosilicate glass," Microelectron. Reliab. **40**, 617–620 (2000).

[32]A. A. Wereszczak and C. E. Anderson, "Borofloat and starphire float glasses: A comparison," Int. J. Appl. Glass Sci. **5**, 334–344 (2014).

[33]C. G. Poulton, R. Pant, and B. J. Eggleton, "Acoustic confinement and stimulated Brillouin scattering in integrated optical waveguides," J. Opt. Soc. Am. B **30**, 2657–2664 (2013).

[34]P. P. Absil, J. V. Hryniewicz, B. E. Little, P. S. Cho, R. A. Wilson, L. G. Joneckis, and P.-T. Ho, "Wavelength conversion in GaAs micro-ring resonators," Opt. Lett. **25**, 554–556 (2000).

[35]A. Kobyakov, M. Sauer, and D. Chowdhury, "Stimulated Brillouin scattering in optical fibers," Adv. Opt. Photonics **2**, 1–59 (2010).

[36]M.-C. Tien, J. F. Bauters, M. J. R. Heck, D. J. Blumenthal, and J. E. Bowers, "Ultra-low loss Si$_3$N$_4$ waveguides with low nonlinearity and high power handling capability," Opt. Express **18**, 23562–23568 (2010).

[37]C. Krückel, V. Torres-Company, P. Andrekson, J. Bovington, J. Bauters, M. Heck, and J. Bowers, "Wavelength conversion in low loss Si$_3$N$_4$ waveguides," in *Conference on Lasers and Electro-Optics (CLEO)* (IEEE, 2014).

[38]X. Zhang, Y. Zhang, C. Xiong, and B. J. Eggleton, "Correlated photon pair generation in low-loss double-stripe silicon nitride waveguides," J. Opt. **18**, 074016 (2016).

11 July 2023 10:55:40